

BayesAdapter: Being Bayesian, Inexpensively and Reliably, via Bayesian Fine-tuning

Zhijie Deng¹ Hao Zhang² Xiao Yang¹ Yinpeng Dong¹ Jun Zhu¹

Abstract

Despite their theoretical appealingness, Bayesian neural networks (BNNs) are left behind in real-world adoption, due to persistent concerns on their scalability, accessibility, and reliability. In this work, we aim to relieve these concerns by developing the *BayesAdapter* framework for learning variational BNNs. In particular, we propose to adapt the pre-trained deterministic NNs to be BNNs via cost-effective *Bayesian fine-tuning*. To make *BayesAdapter* more practical, we technically contribute 1) a modularized, user-friendly implementation for the learning of variational BNNs under two representative variational distributions, 2) a generally applicable strategy for reducing the gradient variance in stochastic variational inference, 3) an explanation for the unreliability issue of BNNs’ uncertainty estimates, and a corresponding prescription. Through extensive experiments on diverse benchmarks, we show that *BayesAdapter* can consistently induce posteriors with higher quality than the from-scratch variational inference and other competitive baselines, especially in large-scale settings, yet significantly reducing training overheads.

1. Introduction

Much effort has been devoted to developing flexible and efficient Bayesian deep models to make accurate, robust, and well-calibrated decisions (MacKay, 1992; Neal, 1995; Graves, 2011; Blundell et al., 2015), with Bayesian neural networks (BNNs) as popular examples. The principled uncertainty quantification inside BNNs is critical for realistic decision-making, finding applications in scenarios ranging from model-based reinforcement learning (Depeweg et al.,

2016), active learning (Hernández-Lobato & Adams, 2015) to healthcare (Leibig et al., 2017) and autonomous driving (Kendall & Gal, 2017). BNNs are also known to be capable of resisting over-fitting.

Nonetheless, BNNs are falling far behind in terms of adoption in real-world applications compared with deterministic NNs (He et al., 2016; Vaswani et al., 2017; Deng et al., 2019), attributing to a variety of practicability issues. For example, the scalability of BNNs is typically limited by the difficulties of learning a complex, non-degenerate distribution from scratch in the high-dimensional parameter space containing many symmetries (Liu & Wang, 2016; Louizos & Welling, 2017; Sun et al., 2019). Implementing a BNN algorithm requires substantial more expertise than implementing a deterministic NN program. Moreover, as revealed, BNNs trained without the “cold posterior” trick are often systematically worse than their point-estimate counterparts in terms of predictive performance (Wenzel et al., 2020a); some easy-to-use BNNs (e.g., Monte Carlo dropout) tend to suffer from mode collapse in function space, thus usually give uncertainty estimates of poor fidelity (Fort et al., 2019).

To mitigate these issues, we introduce a new, pre-training & fine-tuning workflow into the learning of variational BNNs (Blundell et al., 2015), motivated by the inherent connections between variational BNNs and regular deep neural networks (DNNs). The resultant *BayesAdapter* framework learns a variational BNN by performing several rounds of *Bayesian fine-tuning*, starting from a corresponding pre-trained deterministic DNN. Such a paradigm enables us to learn a variational BNN with marginally more effort than training a deterministic NN, but opens up opportunities to embrace a variety of off-the-shelf pre-trained DNNs (e.g., those on PyTorch Hub). The converged parameters of the deterministic model serve as a strong start point for *Bayesian fine-tuning*, allowing to discover qualified function modes more easily than the from-scratch Bayesian learning.

To make *Bayesian fine-tuning* more accessible, we provide an easy-to-use implementation for the learning of variational BNNs under two representative variational distributions: mean-field Gaussian and parameter-sharing ensemble. To stabilize the stochastic optimization, we devise a general-purpose gradient variance reduction strategy named *exem-*

¹Department of Computer Science and Technology, BN-Rist Center, Institute for AI, Tsinghua-Bosch Joint ML Center, THBI Lab, Tsinghua University, Beijing, 100084, China. ²The Robotics Institute, Carnegie Mellon University. Correspondence to: Zhijie Deng <dzj17@mails.tsinghua.edu.cn>, Jun Zhu <dc-szj@tsinghua.edu>.

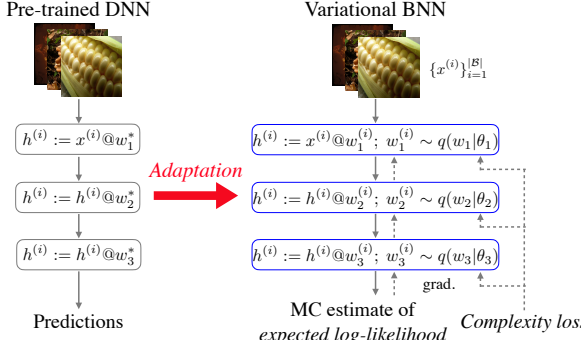


Figure 1. The workflow of *BayesAdapter*: we adapt the pre-trained DNNs to be variational BNNs and then perform *Bayesian fine-tuning*. To render the ELBO maximization (detailed in Eq. (2)) more accessible, we provide a modularized, user-friendly implementation to enable the users to learn a variational BNN as if one were training a regular DNN under weight decay regularizer. To reduce the variance of stochastic gradients, we further develop the *exemplar reparameterization* technique, which deploys a dedicated parameter sample for every exemplar in the mini-batch.

plar reparametrization. Based on these designs, we perform an investigation on the quality of the acquired Bayesian posteriors, and show that typical variational BNNs can seldom yield calibrated uncertainty estimates on realistic, malicious out-of-distribution (OOD) data. As a solution, we opt to explicitly regularize the variational BNNs to behave uncertainly on a collection of OOD data during *Bayesian fine-tuning*. This regularization takes the form of a margin loss, and is readily applicable to most of the existing BNNs. Figure 1 depicts our whole framework.

We conduct extensive experiments to validate the advantages of *Bayesian fine-tuning* over from-scratch approximate Bayesian inference, in aspects covering the learning efficiency, the predictive performance, and the quality of uncertainty estimates of the learned models. We further scale up *BayesAdapter* to large datasets, e.g., ImageNet (Deng et al., 2009), deep architectures, e.g., ResNets (He et al., 2016), and practical scenarios, e.g., face recognition (Deng et al., 2019), and observe competitive results. At last, we perform a series of ablation studies to reveal the characteristics of the proposed approach.

2. BayesAdapter

In this section, we first motivate *BayesAdapter* by drawing a connection between variational BNNs and DNNs under *maximum a posteriori* (MAP) estimation. We then describe the rationale of *Bayesian fine-tuning*, as well as two practical and robust implementations of it. Figure 1 illustrates the overall workflow of *BayesAdapter*.

2.1. From DNNs to BNNs

Let $\mathcal{D} = \{(\mathbf{x}^{(i)}, y^{(i)})\}_{i=1}^n$ be a given training set, where $\mathbf{x}^{(i)} \in \mathbb{R}^d$ and $y^{(i)} \in \mathcal{Y}$ denote the input data and label,

respectively. A DNN model can be fit via MAP as follows:

$$\max_{\mathbf{w}} \frac{1}{n} \sum_i [\log p(y^{(i)} | \mathbf{x}^{(i)}; \mathbf{w})] + \frac{1}{n} \log p(\mathbf{w}). \quad (1)$$

We use $\mathbf{w} \in \mathbb{R}^p$ to denote the high-dimensional model parameters, and $p(y|\mathbf{x}; \mathbf{w})$ as the predictive distribution associated with the model. The prior term $p(\mathbf{w})$, when taking the form of an isotropic Gaussian $\mathcal{N}(\mathbf{w}; \mathbf{0}, \sigma_0^2 \mathbf{I})$, reduces to the common weight decay regularizer with coefficient $\lambda = 1/(\sigma_0^2 n)$ in optimization. Despite wide adoption, DNNs are known to be prone to over-fitting and generating over-confident predictions, and they cannot convey valuable information on the trustworthiness of their predictions. Naturally, Bayesian neural networks (BNNs) come into the picture to address these limitations.

Typically, a BNN imposes a prior $p(\mathbf{w})$ on model parameters, which is put together with the likelihood $p(\mathcal{D}|\mathbf{w})$ to infer the posterior $p(\mathbf{w}|\mathcal{D})$. Among the wide spectrum of BNN algorithms (MacKay, 1992; Neal, 1995; Graves, 2011; Blundell et al., 2015; Liu & Wang, 2016; Gal & Ghahramani, 2016; Louizos & Welling, 2017), variational BNNs are particularly promising due to their ease of training compared with other BNN variants. Formally, variational BNNs derive a θ -parameterized variational distribution $q(\mathbf{w}|\theta)$ to approximate the true posterior $p(\mathbf{w}|\mathcal{D})$, by maximizing the evidence lower bound (ELBO) (scaled by $1/n$):

$$\max_{\theta} \mathbb{E}_{q(\mathbf{w}|\theta)} \left[\underbrace{\frac{1}{n} \sum_i \log p(y^{(i)} | \mathbf{x}^{(i)}; \mathbf{w})}_{\mathcal{L}_{\text{ell}}} - \underbrace{\frac{1}{n} D_{\text{KL}}(q(\mathbf{w}|\theta) || p(\mathbf{w}))}_{\mathcal{L}_{\text{c}}} \right], \quad (2)$$

where \mathcal{L}_{ell} is the *expected log-likelihood* and \mathcal{L}_{c} is the *complexity loss*. By casting posterior inference into optimization, Eq. (2) makes the training of BNNs more approachable. After training, the variational posterior is leveraged for prediction by marginalizing over all likely modes:

$$p(y|\mathbf{x}, \mathcal{D}) = \mathbb{E}_{q(\mathbf{w}|\theta)} p(y|\mathbf{x}; \mathbf{w}) \approx \frac{1}{S} \sum_{s=1}^S p(y|\mathbf{x}; \mathbf{w}^{(s)}), \quad (3)$$

where $\mathbf{w}^{(s)} \sim q(\mathbf{w}|\theta)$, $s = 1, \dots, S$, with S denoting the number of Monte Carlo (MC) samples. Eq. (3) is also known as *posterior predictive* or *Bayes ensemble*.

We can simultaneously quantify the *epistemic* uncertainty with these MC samples. A principled uncertainty metric is the mutual information between the model parameter and the prediction (Smith & Gal, 2018), estimated by:

$$\mathcal{I}(\mathbf{w}, y|\mathbf{x}, \mathcal{D}) \approx H \left(\frac{1}{S} \sum_{s=1}^S p(y|\mathbf{x}; \mathbf{w}^{(s)}) \right) - \frac{1}{S} \sum_{s=1}^S H \left(p(y|\mathbf{x}; \mathbf{w}^{(s)}) \right), \quad (4)$$

where H is the Shannon entropy.

However, most of the existing variational BNNs exhibit limitations in scalability and performance (Osawa et al., 2019; Wenzel et al., 2020a) compared with their deterministic counterparts, fundamentally attributed to the higher

Algorithm 1 Bayesian fine-tuning. Differences from the typical training of DNNs are highlighted.

```

1: Input:  $\mathcal{D}$ : Dataset;  $T$ : Number of epochs;  $\lambda$ : weight decay coefficient
2: Randomly initialize DNN parameters  $\Rightarrow$  Initialize the parameters of the variational BNN with their pre-trained DNN counterparts.
3: for epoch = 1 to  $T$  do
4:   for mini-batch  $\mathcal{B}$  in  $\mathcal{D}$  do
5:     Compute the log-likelihood in Eq. (1)  $\Rightarrow$  Compute the MC estimate of the expected log-likelihood via Eq. (8)
6:     Launch automatic back-propagation
7:     Edit the gradients of DNN parameters in light of vanilla weight decay with coefficient  $\lambda$   $\Rightarrow$  Edit the gradients of variational parameters in light of Eq. (5) (for MFG) or Eq. (6) (for PSE) with coefficient  $\lambda$ 
8:     Perform one-step gradient ascent
9:   end for
10: end for

```

difficulty of learning high-dimensional distributions from scratch than point estimates.

Given that MAP converges to a mode of the Bayesian posterior, it might be plausible to *adapt pre-trained deterministic DNNs to be Bayesian economically*. Following this hypothesis, we repurpose the converged parameters \mathbf{w}^* of MAP – take \mathbf{w}^* as the initialization of the parameters of the approximate posterior. Laplace approximation (Bleistein & Handelsman, 1986) is a classic method in this spirit, which assumes a Gaussian posterior, and adapts \mathbf{w}^* and the local curvature at \mathbf{w}^* as the posterior mean and variance, respectively. Yet, Laplace approximation has two limitations: 1) it is more like a postprocessing, lacking the flexibility to jointly adapt the mean and covariance of the Gaussian posterior w.r.t. data; 2) its naive implementation without strong assumptions may be computationally prohibitive. We remedy these issues by developing the more practical *Bayesian fine-tuning* scheme, whose core notion is to fine-tune the imperfect variational posterior by maximizing ELBO. Algorithm 1 gives an overview of *Bayesian fine-tuning*.

2.2. Bayesian Fine-tuning

In *Bayesian fine-tuning*, the configuration of the variational distribution $q(\mathbf{w}|\theta)$ plays a decisive role. Although a wealth of expressive and flexible variational distributions have emerged for adoption (Louizos & Welling, 2016; Li & Turner, 2017; Wen et al., 2018), on one hand, more complicated ones like multiplicative normalizing flows (Louizos & Welling, 2017) and implicit distributions (Shi et al., 2018b) are routinely accompanied by less scalable and less amenable learning procedures; on the other hand, the aforementioned hypothesis inspiring *Bayesian fine-tuning* entails an explicit alignment between the DNN parameters \mathbf{w}^* and the variational parameters θ . Consequently, we at first place our attention on the typical mean-field Gaussian variational.

Mean-field Gaussian (MFG) variational. Without losing generality, we write the *MFG* variational as $q(\mathbf{w}|\theta) = \mathcal{N}(\mathbf{w}; \boldsymbol{\mu}, \text{diag}(\exp(2\psi)))$, with $\boldsymbol{\mu}, \psi \in \mathbb{R}^p$ denoting the mean and the logarithm of standard deviation respectively. In this sense, we can naturally initialize $\boldsymbol{\mu}$ with \mathbf{w}^* at the

beginning of fine-tuning to ease the approximate posterior inference and to enable the investigation of more qualified posterior modes. As in MAP, we also assume an isotropic Gaussian prior $p(\mathbf{w}) = \mathcal{N}(\mathbf{w}; \mathbf{0}, \sigma_0^2 \mathbf{I})$. Then the gradients of the *complexity loss* can be derived analytically:

$$\nabla_{\boldsymbol{\mu}} \mathcal{L}_c = -\lambda \boldsymbol{\mu}, \quad \nabla_{\psi} \mathcal{L}_c = -\lambda \exp(2\psi) + \frac{1}{n}. \quad (5)$$

Intuitively, the above gradients for the variational parameters correspond to a variant of the *vanilla weight decay*, with λ also equaling to $1/(\sigma_0^2 n)$. Having identified this, we can simply perform gradient editing, in analogy to what *vanilla weight decay* does in the typical training of DNNs, to implicitly be responsible for the *complexity loss* \mathcal{L}_c , leaving only the *expected log-likelihood* \mathcal{L}_{ell} required to be explicitly handled. The rationale of solving $\max \mathcal{L}_{\text{ell}}$ is by Monte Carlo estimation, and we will elaborate the details after presenting a more expressive variational configuration.

Parameter-sharing ensemble (PSE) variational. Despite simplicity, the *MFG* variational is frequently criticized for its too limited expressiveness to account for the multi-modal parameter posterior of over-parameterized neural networks. Empowered by the observation that Deep Ensemble (Lakshminarayanan et al., 2017) is a qualified but expensive BNN method, we intend to develop a low-cost ensemble-like variational for more practical Bayesian deep learning. To this end, we explore a valuable insight from pioneering works on ensemble learning (Wen et al., 2020; Wenzel et al., 2020b) that the parameters of different ensemble candidates can be partially shared to conjoin efficiency and effectiveness.

Specifically, abusing \mathbf{w} to notate the parameter matrix of size $m_{\text{in}} \times m_{\text{out}}$ in a neural network layer¹, we generate C candidate parameters via: $\mathbf{w}^{(c)} = \mathbf{l}^{(c)} \mathbf{r}^{(c)} \circ \bar{\mathbf{w}}$, $c = 1, \dots, C$, where $\bar{\mathbf{w}} \in \mathbb{R}^{m_{\text{in}} \times m_{\text{out}}}$ is the shared parameters, with $\mathbf{l}^{(c)} \in \mathbb{R}^{m_{\text{in}} \times r}$ and $\mathbf{r}^{(c)} \in \mathbb{R}^{r \times m_{\text{out}}}$ corresponding to a r -rank decomposition of some candidate-specialized parameter perturbation. \circ is the element-wise multiplication. When the rank r is suitably small, the above design can significantly reduce the model size, and save the training effort.

¹It is known that the multidimensional convolutional kernel can be converted to an equivalent parameter matrix.

Of note that the previous works (Wen et al., 2020; Wenzel et al., 2020b) confine r to be 1 to permit the adoption of a specialized gradient variance reduction trick. Conversely, we loosen this constraint and develop a more generally applicable variance reduction tactic, which will be detailed later.

We can then formally write the *PSE* variational as $q(\mathbf{w}|\theta) = \frac{1}{C} \sum_{c=1}^C \delta(\mathbf{w} - \mathbf{l}^{(c)} \mathbf{r}^{(c)} \circ \bar{\mathbf{w}})$ (for one NN layer here), where δ denotes the Dirac delta function. The shared parameters $\bar{\mathbf{w}}$ can be initialized as \mathbf{w}^* to ease and speedup the *Bayesian fine-tuning*. Also assuming an isotropic Gaussian prior, we can trivially derive the gradients of the *complexity loss* \mathcal{L}_c :

$$\begin{aligned}\nabla_{\bar{\mathbf{w}}} \mathcal{L}_c &= -\frac{\lambda}{C} \sum_{c=1}^C (\mathbf{l}^{(c)} \mathbf{r}^{(c)}) \circ (\mathbf{l}^{(c)} \mathbf{r}^{(c)}) \circ \bar{\mathbf{w}}, \\ \nabla_{\mathbf{l}^{(c)}} \mathcal{L}_c &= -\frac{\lambda}{C} \left((\mathbf{l}^{(c)} \mathbf{r}^{(c)}) \circ \bar{\mathbf{w}} \circ \bar{\mathbf{w}} \right) \left(\mathbf{r}^{(c)} \right)^\top, \\ \nabla_{\mathbf{r}^{(c)}} \mathcal{L}_c &= -\frac{\lambda}{C} \left(\mathbf{l}^{(c)} \right)^\top \left((\mathbf{l}^{(c)} \mathbf{r}^{(c)}) \circ \bar{\mathbf{w}} \circ \bar{\mathbf{w}} \right).\end{aligned}\quad (6)$$

These gradients can also be absorbed by a weight decay like gradient editing operator. We then only need to explicitly estimate \mathcal{L}_{ell} , rendering the proposed approach modularized.

Robust estimation of the expected log-likelihood \mathcal{L}_{ell} . Given the high non-linearity of the neural networks and the large amount of data in real-world settings, we need to combine Monte Carlo (MC) estimation with stochastic gradient descent to approximately compute \mathcal{L}_{ell} . Formally, given a mini-batch of data $\mathcal{B} = \{(\mathbf{x}^{(i)}, y^{(i)})\}_{i=1}^{|\mathcal{B}|}$, we solve

$$\max_{\theta} \mathcal{L}'_{ell} = \frac{1}{|\mathcal{B}|} \sum_{i=1}^{|\mathcal{B}|} \log p(y^{(i)} | \mathbf{x}^{(i)}; \mathbf{w}), \quad (7)$$

where \mathbf{w} is drawn from the *MFG* or *PSE* variational via reparameterization (Kingma & Welling, 2013). The gradients w.r.t. the variational parameters can be derived automatically with autodiff libraries, thus the training resembles that of regular DNNs.

However, gradients derived by \mathcal{L}'_{ell} might exhibit high variance, caused by sharing the sampled parameters \mathbf{w} across all the training instances in \mathcal{B} . Local reparameterization has been proposed to reduce the variance, but it is typically limited to exponential family and requires at least 2x forward-backward FLOPS compared to vanilla reparameterization (Kingma et al., 2015). Flipout (Wen et al., 2018) is an alternative solution, but it also works under strong assumptions, e.g., the MC estimation is based on symmetric perturbations, thus cannot handle structured distributions like the proposed *PSE* variational. To mitigate these issues, we propose a generic variance reduction technique named *exemplar reparametrization* (ER), which samples dedicated parameters for every exemplar in the minibatch \mathcal{B} . In our case, for $i = 1, \dots, |\mathcal{B}|$, we draw i.i.d. parameter samples $\mathbf{w}^{(i)} = \boldsymbol{\mu} + \exp(\boldsymbol{\psi}) \boldsymbol{\epsilon}^{(i)}$ with $\boldsymbol{\epsilon}^{(i)} \sim \mathcal{N}(\mathbf{0}, \mathbf{I})$ for *MFG*, or $\mathbf{w}^{(i)} = \mathbf{l}^{(c_i)} \mathbf{r}^{(c_i)} \circ \bar{\mathbf{w}}$ with $c_i \sim \text{Uniform}\{1, \dots, C\}$ for *PSE*.

```
# assume shape x: [b, i, h, w]; w: [o, i, k, k]
# theta denotes the variational parameters
def DNN_conv(x, w, stride, padding, groups):
    return conv2d(x, w, stride, padding, groups)

def BayesAdapter_conv(x, theta, stride, padding, groups):
    b = x.shape[0]
    # sample a batch of parameters w: [b, o, i, k, k]
    w = mc_sample(theta, num_mc_samples=b)
    # reshape w to have shape [b*o, i, k, k]
    w = w.flatten(start_dim=0, end_dim=1)
    # reshape x to have shape [1, b*i, h, w]
    x = x.flatten(start_dim=0, end_dim=1).unsqueeze(0)
    # perform b convs in parallel
    y = conv2d(x, w, stride, padding, groups*b)
    # reshape the result to standard format
    return y.view(b, -1, y.shape[2], y.shape[3])
```

Figure 2. The comparison between standard convolution and convolution used in *BayesAdapter*.

We then approximate the *expected log-likelihood* by

$$\mathcal{L}_{ell}^* = \frac{1}{|\mathcal{B}|} \sum_{i=1}^{|\mathcal{B}|} \log p(y^{(i)} | \mathbf{x}^{(i)}; \mathbf{w}^{(i)}). \quad (8)$$

While ER generates more parameters at training, they are temporary, and the resultant computational FLOPS are provably identical to that of the vanilla reparameterization. The challenge of ER is to cope with nowadays ML frameworks and maintain computing efficiency, because off-the-shelf computation kernels typically proceed by sharing parameters among the data in a mini-batch. We present an example in Figure 2 on how the standard convolution op can be converted into its exemplar version without compromising computational efficiency. The key insight here is that multiple exemplar convolutions can be expressed as a group convolution, which can be performed in parallel using a single group convolution kernel, leveraging the optimized implementations provided by various device-proprietary kernel backends (e.g. cuDNN (Chetlur et al., 2014)). Other common operators such as matrix multiplication are straightforward to handle (refer to Appendix A).

We wrap the details of the aforementioned weight decay like gradient editing and ER strategy for the two variational in a plug-and-play Python library (attached in supplementary materials) to conceivably free the users from the difficulties of implementing *Bayesian fine-tuning*.

3. Calibrate the Predictive Uncertainty

Based on the efficient *Bayesian fine-tuning* paradigm, we can perform faster learning of BNNs, and hence deeper investigations on the quality of Bayesian posteriors. Given some evidence that BNNs are likely to assign undesirably low *epistemic* uncertainty for adversarial examples (Grosse et al., 2018), we particularly concern the uncertainty estimates yielded by the learned BNNs for realistic, malicious out-of-distribution (OOD) data, to make clear the usefulness of BNNs in real-world scenarios.

We conduct a diagnostic qualitative assessment in two challenging scenarios: CIFAR-10 (Krizhevsky et al., 2009) and ImageNet (Deng et al., 2009) classification, where the ad-

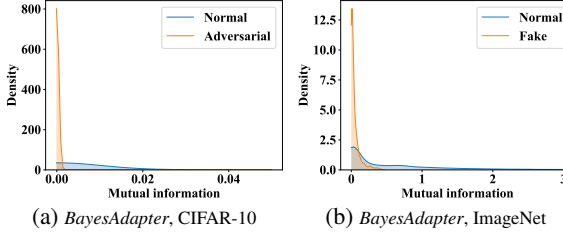


Figure 3. The histograms for the mutual information uncertainty of normal data and OOD data given by *BayesAdapter* (*MFG*).

versarial examples from PGD attack (Madry et al., 2017) and the fake samples from BigGAN (Brock et al., 2018) are collected as OOD data, respectively. We experiment with *MFG* here while *PSE* behaves similarly. More details are deferred to Sec 4. We plot the histograms for the estimated uncertainty of normal data and OOD data in Figure 6.

It is evident that the two kinds of OOD data tends to be assigned systematically lower uncertainty than normal data, implying that the predictive uncertainty of typical variational BNNs is probably unreliable and misleading in practical safety-critical scenarios. To address this problem, we suggest to calibrate the predictive uncertainty on top of the ELBO maximization during *Bayesian fine-tuning*.

Basically, we regularize the BNNs to give high uncertainty for a cheap collection of OOD data, so that they acquire the ability of yielding high uncertainty for unseen OOD samples with similar fingerprints. Namely, assuming access to some OOD data $\{\mathbf{x}_0^{(i)}\}_{i=1}^{n_0}$, we optimize the following margin loss:

$$\max_{\theta} \mathcal{L}_{reg} = \frac{1}{|\mathcal{B}_0|} \sum_{\mathbf{x}_0^{(i)} \in \mathcal{B}_0} \min \left(\mathcal{I}(\mathbf{w}, y | \mathbf{x}_0^{(i)}, \mathcal{D}), \gamma \right), \quad (9)$$

where \mathcal{B}_0 refers to a mini-batch of OOD data and γ is the threshold. For efficiency, we adopt $S = 2$ MC samples for estimating the uncertainty \mathcal{I} in Eq. (9) during training. The overall objective for *BayesAdapter w/ reg* is then $\mathcal{L}_{ell}^* + \alpha \mathcal{L}_{reg}$ with α representing a trade-off coefficient. While \mathcal{L}_{reg} has a seemingly opposite form from the consistency-promoting loss in semi-supervised learning (SSL) (Laine & Aila, 2016), they share similar design philosophy: \mathcal{L}_{reg} maximizes the prediction inconsistency of OOD data so as to distinguish them from normal data, while SSL minimizes the prediction inconsistency of unlabeled instances to exploit the valuable information inside them.

For empirical verification, we deploy *BayesAdapter w/ reg* to the two aforementioned settings. We take uniformly contaminated samples, which serve as a proxy of the expensive adversarial examples crafted by PGD, and 1000 BigGAN samples as the training OOD data for CIFAR-10 and ImageNet respectively. The results are presented in Figure 4. As expected, *BayesAdapter w/ reg* succeeds to behave uncertainly on the challenging OOD test data, exhibiting significantly improved practicability over vanilla

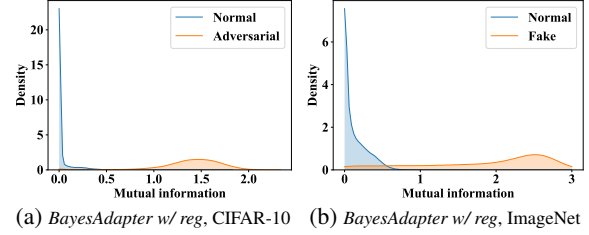


Figure 4. The histograms for the mutual information uncertainty of normal data and OOD data given by *BayesAdapter w/ reg* (*MFG*).

Bayesian learning. For example, *BayesAdapter w/ reg* can reject to predict for risky OOD data more robustly. This empirical study also testifies that the regularization \mathcal{L}_{reg} is data efficient.

4. Experiments

In this section, we apply *BayesAdapter* to a diverse set of challenging benchmarks to demonstrate its benefits.

Settings. In general, we pre-train DNNs following standard protocols or fetch the pre-trained checkpoints available online, and then perform *Bayesian fine-tuning* using the two developed variationals. We randomly initialize the newly added variational parameters (e.g., ψ , $\mathbf{l}^{(c)}$, $\mathbf{r}^{(c)}$). Unless otherwise stated, we set rank $r = 1$ and candidate number $C = 20$ for *PSE*. We use $S = 20$ MC samples for predicting and quantifying uncertainty for both *MFG* and *PSE*. For *BayesAdapter w/ reg*, We set $\alpha = 3$ without tuning and set uncertainty threshold $\gamma = 0.75$ according to an observation that the normal examples usually present < 0.75 mutual information uncertainty across various scenarios. Full details are deferred to Appendix B. We run per experiment for 3 times on 8 RTX 2080-TIs and report the average as well as the error bar.

Baselines. We consider extensive baselines including: (1) *MAP*, which is the fine-tuning start point, (2) *Laplace Approx.*: which performs Laplace approximation with diagonal Fisher information matrix, (3) *MC dropout*, which is a dropout variant of *MAP*, (4) *VBNN*, which refers to from-scratch trained variational BNNs under ELBO maximization. In particular, the variational BNN methods like *BayesAdapter* and *VBNN* are evaluated on both the *MFG* and *PSE* variational. We also include *Deep Ensemble* (Lakshminarayanan et al., 2017), one of the state-of-the-art BNNs, and *SWAG* (Maddox et al., 2019), whose performance is not worse than SGLD (Welling & Teh, 2011), KFAC Laplace (Ritter et al., 2018) and temperature scaling (Guo et al., 2017), into the comparison on CIFAR-10².

Quantitative measure for the quality of predictive uncertainty. We estimate the predictive uncertainty of the trained models on normal data as well as realistic OOD data,

²Currently, we have not scaled *Deep Ensemble* and *SWAG* up to ImageNet due to resource constraints.

Table 1. Comparison on predictive performance and quality of uncertainty estimates. NLL denotes the negative log-likelihood. We use underline to emphasize the results obtained given significantly more training effort. (CIFAR-10)

Method	Predictive performance		Quality of uncertainty estimates in terms of AP	
	TOP1 (%) \uparrow	NLL \downarrow	Adversarial (PGD) \uparrow	Fake (SNGAN) \uparrow
<i>MAP</i>	96.92	0.1312	0.307	0.800
<i>Laplace Approx.</i>	96.41	0.1204	0.308	0.800
<i>MC dropout</i>	96.95	0.1151	0.308	0.803
<i>SWAG</i>	96.32	0.1122	0.316	0.816
<i>Deep Ensemble</i>	97.40	0.0869	0.427	0.812
<i>VBNN (MFG)</i>	96.95 ± 0.09	0.0994 ± 0.0028	0.308 ± 0.000	0.813 ± 0.000
<i>VBNN (PSE)</i>	96.88 ± 0.03	0.1328 ± 0.0020	0.309 ± 0.001	0.794 ± 0.005
<i>BayesAdapter (MFG)</i>	97.10 ± 0.03	0.1007 ± 0.0014	0.307 ± 0.001	0.806 ± 0.002
<i>BayesAdapter (PSE)</i>	97.13 ± 0.03	0.0936 ± 0.0010	0.326 ± 0.003	0.814 ± 0.000
<i>BayesAdapter w/ reg (MFG)</i>	96.82 ± 0.07	0.1004 ± 0.0026	0.985 ± 0.005	0.996 ± 0.002
<i>BayesAdapter w/ reg (PSE)</i>	96.86 ± 0.06	0.1173 ± 0.0030	0.783 ± 0.054	0.998 ± 0.001

Table 2. Comparison on predictive performance and quality of uncertainty estimates. (ImageNet)

Method	Predictive performance		Quality of uncertainty estimates in terms of AP	
	TOP1 (%) \uparrow	NLL \downarrow	Adversarial (PGD) \uparrow	Fake (BigGAN) \uparrow
<i>MAP</i>	76.13	0.9618	0.308	0.010
<i>Laplace Approx.</i>	75.89	0.9739	0.311	0.015
<i>MC dropout</i>	74.88	0.9884	0.309	0.012
<i>VBNN (MFG)</i>	75.97	0.9435	0.310	0.021
<i>VBNN (PSE)</i>	75.12	0.9865	0.313	0.013
<i>BayesAdapter (MFG)</i>	76.45 ± 0.05	0.9303 ± 0.0005	0.310 ± 0.000	0.013 ± 0.000
<i>BayesAdapter (PSE)</i>	76.80 ± 0.03	0.9159 ± 0.0010	0.397 ± 0.004	0.014 ± 0.000
<i>BayesAdapter w/ reg (MFG)</i>	76.26 ± 0.06	0.9428 ± 0.0020	0.964 ± 0.009	0.848 ± 0.037
<i>BayesAdapter w/ reg (PSE)</i>	76.48 ± 0.06	0.9752 ± 0.0030	0.976 ± 0.004	0.714 ± 0.017

including adversarial examples crafted by 20-step PGD following standard protocols and fake samples from performant GANs (Miyato et al., 2018; Brock et al., 2018) or DeepFake (see Appendix D for some examples). We then base on the uncertainty to distinguish OOD test data from normal test data and report the average precision (AP) of such a binary classification (i.e., OOD detection) to reflect the quality of predictive uncertainty.

4.1. CIFAR-10 Classification

We first empirically substantiate the superiority of *BayesAdapter* on CIFAR-10 classification with wide-ResNet-28-10 architecture (Zagoruyko & Komodakis, 2016). We perform *Bayesian fine-tuning* for 12 epochs with the weight decay coefficient λ set as 2e-4 following common practice. Table 1 outlines the comparison on prediction performance as well as the that on the quality of predictive uncertainty.

On one hand, *BayesAdapter* notably outperforms *MAP*, *Laplace Approx.*, *MC dropout*, and *SWAG* in aspect of predictive performance, highlighting the practical value of our workflow. The accuracy upper bound is *Deep Ensemble*, which trains 5 isolated *MAPs* and assembles their predictions to explicitly investigate diverse function modes, but it is orders of magnitude more expensive than *BayesAdapter*. *VBNN* is clearly defeated by *BayesAdapter*, confirming our claim that performing *Bayesian fine-tuning* from the converged deterministic checkpoints is beneficial to explore

more qualified posterior modes.

On the other hand, *BayesAdapter w/ reg* significantly surpasses all other methods in aspect of the quality of uncertainty estimates, although the regularization \mathcal{L}_{reg} slightly undermines the performance³. In particular, *Deep Ensemble* also yields unreliable predictive uncertainty for the difficult OOD data. These results echo our concern on the reliability of existing BNNs’ predictive uncertainty and prove the efficacy of the developed uncertainty regularization.

In addition, we notice that the uncertainty estimates of *BayesAdapter w/ reg (PSE)* for detecting OOD data are relatively less calibrated than *BayesAdapter w/ reg (MFG)*. We deduce that this is because once *MFG* approaches a flat high-quality posterior, *MFG* can dedicate its variance parameters to accounting for the uncertainty regularization, while *PSE* needs to find diverse posterior spikes to guarantee both data fittingness and calibrated uncertainty concurrently, which may be more demanding.

Speedup. Based on our implementation, the stochastic variational inference with *PSE* takes around 2 minutes for one epoch on 8 RTX 2080-TIs. Thus, *VBNN* trained from scratch consumes 400 minutes for 200-epoch training, while *BayesAdapter* needs only 24 minutes for 12-epoch fine-tuning, saving 376 minutes (94%) training time than *VBNN*.

³We think this is reasonable since the uncertainty regularization enforces the model to trade partial capacity for the fidelity of uncertainty estimates.

Table 3. Accuracy \uparrow comparison on open-set face recognition with MobileNetV2 architecture.

Method	LFW	CPLFW	CALFW	CFP-FF	CFP-FP	VGGFace2	AgeDB-30
<i>MAP</i>	98.2%	84.0%	87.6%	97.8%	92.7%	91.7%	85.3%
<i>MC dropout</i>	98.2%	83.6%	87.3%	97.8%	92.8%	92.6%	86.0%
<i>BayesAdapter (MFG)</i>	98.4%	83.9%	85.8%	97.6%	92.9%	93.1%	84.5%
<i>BayesAdapter (PSE)</i>	98.4%	84.7%	87.8%	97.8%	93.1%	92.4%	85.7%
<i>BayesAdapter w/ reg (MFG)</i>	98.4%	84.1%	87.4%	97.9%	93.1%	92.5%	84.8%
<i>BayesAdapter w/ reg (PSE)</i>	98.0%	84.1%	87.7%	97.9%	92.6%	92.0%	85.9%

4.2. ImageNet Classification

We then scale up *BayesAdapter* to the large ImageNet dataset with ResNet-50 (He et al., 2016) architecture. We fetch the pre-trained model from PyTorch Hub and launch fine-tuning for merely **4 epochs** with the weight decay coefficient λ set as the popular value $1e-4$.

Table 2 reports the empirical comparison. As expected, most of results are consistent with those on CIFAR-10. On this large-scale scenario with less over-fitting, it is more clear that the from-scratch learning baseline *VBNN* would suffer from local optima. The striking improvement of *BayesAdapter* upon *MAP* validates the benefits of Bayesian treatment. Zooming in, we also note that *BayesAdapter (PSE)* reveals remarkably higher accuracy than the *BayesAdapter (MFG)*, testifying the enhanced expressiveness of *PSE* over *MFG*. On the other side of the spectrum, *BayesAdapter w/ reg* is better than its fine-tuning start point *MAP* and the from-scratch baseline *VBNN* on both axes of comparison, double evidencing the usefulness of the uncertainty regularization and highlighting the practical value of the proposed approach.

4.3. Face Recognition

To demonstrate the universality of *BayesAdapter*, we further apply it to the challenging face recognition task based on MobileNetV2 (Sandler et al., 2018). We train models on the CASIA dataset (Yi et al., 2014), and perform comprehensive evaluation on face verification datasets including LFW (Huang et al., 2007), CPLFW (Zheng & Deng, 2018), CALFW (Zheng et al., 2017), CFP (Sengupta et al., 2016), VGGFace2 (Cao et al., 2018), and AgeDB-30 (Moschoglou et al., 2017). We launch fine-tuning for 4 epochs with $\lambda = 5e-4$. Given the ineffectiveness of the from-scratch learning of variational BNNs and Laplace approximation reflected by the above studies, we mainly compare our method to *MAP* and *MC dropout* here. We depict the comparison on recognition accuracy in Table 3 and that on quality of uncertainty estimates in Table 1 and 2 of Appendix C.

It is noteworthy that Bayesian principle can induce better predictive performance for face recognition models. *BayesAdapter (PSE)* has outperformed the fine-tuning start point *MAP* and the popular baseline *MC dropout* in most verification datasets, despite being fine-tuned for only several rounds. The near-perfect results of *BayesAdapter w/*

Table 4. Comparison on model calibration (ECE \downarrow).

Method	CIFAR-10	ImageNet
<i>MAP</i>	0.0198	0.0373
<i>Laplace Approx.</i>	0.0106	0.0375
<i>MC dropout</i>	0.0119	0.0152
<i>SWAG</i>	0.0088	-
<i>Deep Ensemble</i>	0.0057	-
<i>VBNN (MFG)</i>	0.0074	0.0183
<i>VBNN (PSE)</i>	0.0188	0.0202
<i>BayesAdapter (MFG)</i>	0.0091	0.0289
<i>BayesAdapter (PSE)</i>	0.0058	0.0129

reg for detecting OOD instances signify the potential of the developed approach in industrial applications.

4.4. More Empirical Analyses

Model calibration. Model calibration is another important aspect of the uncertainty estimation. Suggested by pioneering works, we take the *Expected Calibration Error* (ECE) (Guo et al., 2017) as the measure of calibration, and report the ECE of the studied methods⁴ in Table 4. Notably, the ECE of *BayesAdapter (PSE)* is on par with *Deep Ensemble*, significantly better than the other baselines.

The impact of the rank r for *PSE*. As stated, we set $r = 1$ for all the above studies for maximal parameter saving. Yet, does the small rank r confine the expressiveness of *PSE*? We perform an ablation study, which is presented in Table 5, to pursue the answer. As shown, the capacity of *PSE* can already be sufficiently unleashed when the rank is 1. This indicates the merit of *PSE* for efficient learning.

The effectiveness of *exemplar reparameterization*. We build a toy model with only a convolutional layer and fix the model input and the target output. We employ the *MFG* variational on the convolutional parameters and computing the variance of stochastic gradients across 500 runs. We average the gradient variance of μ and ψ over all their coordinates, and observe that standard reparameterization typically introduces more than $100\times$ variance than *exemplar reparameterization*, despite with the same FLOPS.

The impact of the training uncertainty threshold γ . We perform an ablation study regarding γ on CIFAR-10 to evaluate the hyper-parameter tolerance of the uncertainty regularization \mathcal{L}_{reg} . We take *BayesAdapter w/ reg (MFG)*

⁴We exclude *BayesAdapter w/ reg* in this comparison since that the primary goal of the regularization \mathcal{L}_{reg} is to calibrate the *epistemic* uncertainty instead of the predictive confidence.

Table 5. Ablation study on the rank r of PSE. (ImageNet)

Method	TOP1 (%)	# of Param. (M)
MAP	76.13	25.56
BayesAdapter (PSE, $r=1$)	76.80	27.21
BayesAdapter (PSE, $r=8$)	76.78	38.76
BayesAdapter (PSE, $r=16$)	76.80	51.95

 Table 6. Ablation study on the uncertainty threshold γ in \mathcal{L}_{reg} . (BayesAdapter w/ reg (MFG), CIFAR-10)

γ	TOP1 (%)	AP (Adversarial)	AP (Fake)
0.25	96.93%	0.915	0.910
0.50	96.70%	0.948	0.981
0.75	96.82%	0.985	0.996
1.00	96.74%	0.991	0.994
1.50	96.79%	0.944	0.988

for this ablation study due to its effectiveness shown in Table 1 and 2. Table 6 presents the results, which reveal that values of $\gamma \in [0.75, 1.0]$ may be good choices for OOD detection, and also echo the observation that normal examples usually have < 0.75 uncertainty.

The impact of ensemble number. We draw the change of test accuracy w.r.t. the number of MC samples S for *Bayes ensemble* in Figure 5a. The model is trained by *BayesAdapter (MFG)* on ImageNet. The points on the red line represent the individual accuracies of the 100 parameter samples. The yellow dashed line refers to the deterministic inference with only the Gaussian mean. The green line displays the effects of *Bayes ensemble* – the predictive performance increases from $< 74\%$ to $> 76\%$ quickly before seeing 20 parameter samples, and gradually saturate after that. That is why we set $S = 20$ in the above studies.

Uncertainty-based rejective decision. In practice, we expect our models can reject to predict for data with relatively high uncertainty, and only care about the data that they are certain about. In this spirit, we sort the validation data of ImageNet w.r.t. the uncertainty provided by *BayesAdapter (MFG)*, and split them into 10 buckets of equal size. We depict the average accuracy of each bucket in Figure 5b. As expected, our BNN is more accurate for instances with smaller uncertainty. Quantitatively, there are 95% instances with uncertainty less than 0.45, and their accuracy is 78.6%; there are 90% instances with uncertainty less than 0.37, and their accuracy is 80.7%; there are 80% instances with uncertainty less than 0.25, and their accuracy is 84.8%.

5. Related Work

Fruitful works have emerged in the BNN community in the last decade (Graves, 2011; Welling & Teh, 2011; Blundell et al., 2015; Kingma & Welling, 2013; Balan et al., 2015; Liu & Wang, 2016; Kendall & Gal, 2017). However, most of the existing works cannot achieve the goal of practicality. For example, Louizos & Welling (2016; 2017); Shi et al. (2018a); Sun et al. (2019) trade learning efficiency for flexible variational posteriors, leading to restrictive scal-

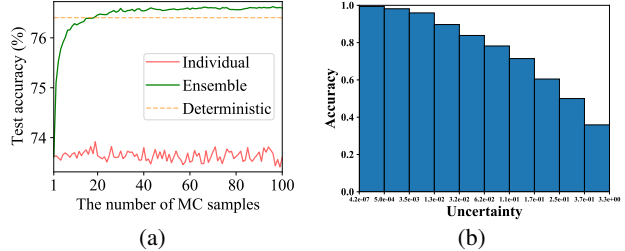


Figure 5. (a): The change of test accuracy w.r.t. the number of MC samples S for *Bayes ensemble*, i.e., Eq. (3). (b): Comparison on the accuracy for instance buckets of equal size but with rising uncertainty. (*BayesAdapter (MFG)*, ImageNet)

ability. Khan et al. (2018); Zhang et al. (2018); Osawa et al. (2019) build Adam-like optimizers to do variational inference, but their parallel training throughput and compatibility with data augmentation are inferior to SGD. Empirical Bayes methods, e.g., Monte Carlo (MC) dropout (Gal & Ghahramani, 2016), deep ensemble (Lakshminarayanan et al., 2017), and SWAG (Maddox et al., 2019), usually maintain impressive predictive performance, but suffer from degenerated uncertainty estimates (Fort et al., 2019) or expensive training/storage cost. What’s worse, the existing works usually evaluate on impractical OOD data (Louizos & Welling, 2017; Pawlowski et al., 2017) to show the merit of Bayesian principle. Instead, we offer a new evaluation standard in this work, which may benefit the following works.

Laplacian approximation (Bleistein & Handelsman, 1986; Ritter et al., 2018) is a known approach to transform a DNN to a BNN, but it is inflexible due to its postprocessing nature and some strong assumptions made for practical concerns. Alternatively, *BayesAdapter* works in the style of fine-tuning, which is more natural and economical for deep networks. Bayesian modeling the last layer of a DNN is proposed recently (Kristiadi et al., 2020), and its combination with *BayesAdapter* deserves an investigation. *BayesAdapter* connects to MOPED (Krishnan et al.) in that their variational configurations are both based on MAP. Yet, beyond MOPED, *BayesAdapter* is further designed to achieve good user-friendliness, improved learning stability, and trustable uncertainty estimation, which are essentially crucial in real-world and large-scale settings.

6. Conclusions

In this work, we propose the scalable *BayesAdapter* framework to learn practical BNNs. Our core idea is to perform *Bayesian fine-tuning* instead of expensive from-scratch Bayesian learning. We develop plug-and-play implementations for the stochastic variational inference under two practical variational distributions, and propose *exemplar reparameterization* to reduce the gradient variance. We also propose a generic uncertainty regularization to calibrate the uncertainty quantification. We evaluate *BayesAdapter* in diverse real-world scenarios and report promising results.

References

Balan, A. K., Rathod, V., Murphy, K. P., and Welling, M. Bayesian dark knowledge. In *Advances in Neural Information Processing Systems*, pp. 3438–3446, 2015.

Bleistein, N. and Handelsman, R. A. *Asymptotic expansions of integrals*. Courier Corporation, 1986.

Blundell, C., Cornebise, J., Kavukcuoglu, K., and Wierstra, D. Weight uncertainty in neural network. In *International Conference on Machine Learning*, pp. 1613–1622, 2015.

Brock, A., Donahue, J., and Simonyan, K. Large scale gan training for high fidelity natural image synthesis. *arXiv preprint arXiv:1809.11096*, 2018.

Cao, Q., Shen, L., Xie, W., Parkhi, O. M., and Zisserman, A. Vggface2: A dataset for recognising faces across pose and age. In *2018 13th IEEE International Conference on Automatic Face & Gesture Recognition (FG 2018)*, pp. 67–74. IEEE, 2018.

Chetlur, S., Woolley, C., Vandermersch, P., Cohen, J., Tran, J., Catanzaro, B., and Shelhamer, E. cudnn: Efficient primitives for deep learning. *arXiv preprint arXiv:1410.0759*, 2014.

Deepfakes, 2018. <https://github.com/deepfakes/faceswap>. Accessed: 2018-10-29.

Deng, J., Dong, W., Socher, R., Li, L.-J., Li, K., and Fei-Fei, L. ImageNet: A Large-Scale Hierarchical Image Database. In *CVPR09*, 2009.

Deng, J., Guo, J., Xue, N., and Zafeiriou, S. Arcface: Additive angular margin loss for deep face recognition. In *Proceedings of the IEEE Conference on Computer Vision and Pattern Recognition*, pp. 4690–4699, 2019.

Depeweg, S., Hernández-Lobato, J. M., Doshi-Velez, F., and Udluft, S. Learning and policy search in stochastic dynamical systems with Bayesian neural networks. *arXiv preprint arXiv:1605.07127*, 2016.

DeVries, T. and Taylor, G. W. Improved regularization of convolutional neural networks with cutout. *arXiv preprint arXiv:1708.04552*, 2017.

Faceswap, 2018. <https://github.com/MarekKowalski/FaceSwap>. Accessed: 2018-10-29.

Fort, S., Hu, H., and Lakshminarayanan, B. Deep ensembles: A loss landscape perspective. *arXiv preprint arXiv:1912.02757*, 2019.

Gal, Y. and Ghahramani, Z. Dropout as a Bayesian approximation: Representing model uncertainty in deep learning. In *International Conference on Machine Learning*, pp. 1050–1059, 2016.

Graves, A. Practical variational inference for neural networks. In *Advances in Neural Information Processing Systems*, pp. 2348–2356, 2011.

Grosse, K., Pfaff, D., Smith, M. T., and Backes, M. The limitations of model uncertainty in adversarial settings. *arXiv preprint arXiv:1812.02606*, 2018.

Guo, C., Pleiss, G., Sun, Y., and Weinberger, K. Q. On calibration of modern neural networks. *arXiv preprint arXiv:1706.04599*, 2017.

He, K., Zhang, X., Ren, S., and Sun, J. Deep residual learning for image recognition. In *Proceedings of the IEEE Conference on Computer Vision and Pattern Recognition*, pp. 770–778, 2016.

Hernández-Lobato, J. M. and Adams, R. Probabilistic back-propagation for scalable learning of Bayesian neural networks. In *International Conference on Machine Learning*, pp. 1861–1869, 2015.

Huang, G. B., Mattar, M., Berg, T., and Learned-Miller, E. Labeled faces in the wild: A database for studying face recognition in unconstrained environments. In *Technical report*, 2007.

Ioffe, S. and Szegedy, C. Batch normalization: Accelerating deep network training by reducing internal covariate shift. *arXiv preprint arXiv:1502.03167*, 2015.

Kendall, A. and Gal, Y. What uncertainties do we need in Bayesian deep learning for computer vision? In *Advances in Neural Information Processing Systems*, pp. 5574–5584, 2017.

Khan, M. E., Nielsen, D., Tangkaratt, V., Lin, W., Gal, Y., and Srivastava, A. Fast and scalable Bayesian deep learning by weight-perturbation in adam. In *International Conference on Machine Learning*, pp. 2616–2625, 2018.

Kingma, D. P. and Welling, M. Auto-encoding variational Bayes. *arXiv preprint arXiv:1312.6114*, 2013.

Kingma, D. P., Salimans, T., and Welling, M. Variational dropout and the local reparameterization trick. In *Advances in Neural Information Processing Systems*, pp. 2575–2583, 2015.

Krishnan, R., Subedar, M., and Tickoo, O. Specifying weight priors in bayesian deep neural networks with empirical bayes.

Kristiadi, A., Hein, M., and Hennig, P. Being bayesian, even just a bit, fixes overconfidence in relu networks. *arXiv preprint arXiv:2002.10118*, 2020.

Krizhevsky, A., Hinton, G., et al. Learning multiple layers of features from tiny images. 2009.

Laine, S. and Aila, T. Temporal ensembling for semi-supervised learning. *arXiv preprint arXiv:1610.02242*, 2016.

Lakshminarayanan, B., Pritzel, A., and Blundell, C. Simple and scalable predictive uncertainty estimation using deep ensembles. In *Advances in Neural Information Processing Systems*, pp. 6402–6413, 2017.

Leibig, C., Allken, V., Ayhan, M. S., Berens, P., and Wahl, S. Leveraging uncertainty information from deep neural networks for disease detection. *Scientific Reports*, 7(1): 1–14, 2017.

Li, Y. and Turner, R. E. Gradient estimators for implicit models. *arXiv preprint arXiv:1705.07107*, 2017.

Liu, Q. and Wang, D. Stein variational gradient descent: A general purpose Bayesian inference algorithm. In *Advances in Neural Information Processing Systems*, pp. 2378–2386, 2016.

Louizos, C. and Welling, M. Structured and efficient variational deep learning with matrix gaussian posteriors. In *International Conference on Machine Learning*, pp. 1708–1716, 2016.

Louizos, C. and Welling, M. Multiplicative normalizing flows for variational Bayesian neural networks. In *International Conference on Machine Learning*, pp. 2218–2227, 2017.

MacKay, D. J. A practical Bayesian framework for back-propagation networks. *Neural Computation*, 4(3):448–472, 1992.

Maddox, W. J., Izmailov, P., Garipov, T., Vetrov, D. P., and Wilson, A. G. A simple baseline for bayesian uncertainty in deep learning. In *Advances in Neural Information Processing Systems*, pp. 13153–13164, 2019.

Madry, A., Makelov, A., Schmidt, L., Tsipras, D., and Vladu, A. Towards deep learning models resistant to adversarial attacks. *arXiv preprint arXiv:1706.06083*, 2017.

Miyato, T., Kataoka, T., Koyama, M., and Yoshida, Y. Spectral normalization for generative adversarial networks. *arXiv preprint arXiv:1802.05957*, 2018.

Moschoglou, S., Papaioannou, A., Sagonas, C., Deng, J., Kotsia, I., and Zafeiriou, S. Agedb: the first manually collected, in-the-wild age database. In *Proceedings of the IEEE Conference on Computer Vision and Pattern Recognition Workshops*, pp. 51–59, 2017.

Neal, R. M. *Bayesian Learning for Neural Networks*. PhD thesis, University of Toronto, 1995.

Osawa, K., Swaroop, S., Jain, A., Eschenhagen, R., Turner, R. E., Yokota, R., and Khan, M. E. Practical deep learning with Bayesian principles. *arXiv preprint arXiv:1906.02506*, 2019.

Pawlowski, N., Brock, A., Lee, M. C., Rajchl, M., and Glocker, B. Implicit weight uncertainty in neural networks. *arXiv preprint arXiv:1711.01297*, 2017.

Ritter, H., Botev, A., and Barber, D. A scalable laplace approximation for neural networks. In *6th International Conference on Learning Representations, ICLR 2018-Conference Track Proceedings*, volume 6. International Conference on Representation Learning, 2018.

Sandler, M., Howard, A., Zhu, M., Zhmoginov, A., and Chen, L.-C. Mobilenetv2: Inverted residuals and linear bottlenecks. In *Proceedings of the IEEE conference on computer vision and pattern recognition*, pp. 4510–4520, 2018.

Sengupta, S., Chen, J.-C., Castillo, C., Patel, V. M., Chellappa, R., and Jacobs, D. W. Frontal to profile face verification in the wild. In *2016 IEEE Winter Conference on Applications of Computer Vision (WACV)*, pp. 1–9. IEEE, 2016.

Shi, J., Sun, S., and Zhu, J. Kernel implicit variational inference. In *International Conference on Learning Representations*, 2018a.

Shi, J., Sun, S., and Zhu, J. A spectral approach to gradient estimation for implicit distributions. *arXiv preprint arXiv:1806.02925*, 2018b.

Smith, L. and Gal, Y. Understanding measures of uncertainty for adversarial example detection. *arXiv preprint arXiv:1803.08533*, 2018.

Sun, S., Zhang, G., Shi, J., and Grosse, R. Functional variational Bayesian neural networks. In *International Conference on Learning Representations*, 2019.

Thies, J., Zollhofer, M., Stamminger, M., Theobalt, C., and Niebner, M. Face2face: Real-time face capture and reenactment of rgb videos. In *Proceedings of the IEEE Conference on Computer Vision and Pattern Recognition*, pp. 2387–2395, 2016.

Vaswani, A., Shazeer, N., Parmar, N., Uszkoreit, J., Jones, L., Gomez, A. N., Kaiser, Ł., and Polosukhin, I. Attention is all you need. In *Advances in neural information processing systems*, pp. 5998–6008, 2017.

Welling, M. and Teh, Y. W. Bayesian learning via stochastic gradient langevin dynamics. In *Proceedings of the 28th international conference on machine learning (ICML-11)*, pp. 681–688, 2011.

Wen, Y., Vicol, P., Ba, J., Tran, D., and Grosse, R. Flipout: Efficient pseudo-independent weight perturbations on mini-batches. *arXiv preprint arXiv:1803.04386*, 2018.

Wen, Y., Tran, D., and Ba, J. Batchensemble: an alternative approach to efficient ensemble and lifelong learning. *arXiv preprint arXiv:2002.06715*, 2020.

Wenzel, F., Roth, K., Veeling, B. S., Swiatkowski, J., Tran, L., Mandt, S., Snoek, J., Salimans, T., Jenatton, R., and Nowozin, S. How good is the bayes posterior in deep neural networks really? *arXiv preprint arXiv:2002.02405*, 2020a.

Wenzel, F., Snoek, J., Tran, D., and Jenatton, R. Hyperparameter ensembles for robustness and uncertainty quantification. *arXiv preprint arXiv:2006.13570*, 2020b.

Yi, D., Lei, Z., Liao, S., and Li, S. Z. Learning face representation from scratch. *arXiv preprint arXiv:1411.7923*, 2014.

Zagoruyko, S. and Komodakis, N. Wide residual networks. *arXiv preprint arXiv:1605.07146*, 2016.

Zhang, G., Sun, S., Duvenaud, D., and Grosse, R. Noisy natural gradient as variational inference. In *International Conference on Machine Learning*, pp. 5847–5856, 2018.

Zheng, T. and Deng, W. Cross-pose lfw: A database for studying cross-pose face recognition in unconstrained environments. *Beijing University of Posts and Telecommunications, Tech. Rep*, 5, 2018.

Zheng, T., Deng, W., and Hu, J. Cross-age lfw: A database for studying cross-age face recognition in unconstrained environments. *arXiv preprint arXiv:1708.08197*, 2017.

A. The Exemplar Version of Popular Operators

As introduced in Sec 2.2, the regular convolution can be elegantly converted into an exemplar version by resorting to group convolution. The other popular operators are relatively easy to handle. For example, we substitute the qualified batch matrix multiplication, which is highly optimized in the well-known autodiff libraries, for matrix multiplication. For the affine transformation in batch normalization (Ioffe & Szegedy, 2015), we can at first sample dedicated affine weight and bias for every exemplar in the batch, then perform transformation with these two batches of parameters by just not *broadcasting* on the batch dimension.

B. More Experimental Details

The only two important hyper-parameters are the weight decay coefficient λ and the uncertainty threshold γ . Other hyper-parameters for defining PGD or specifying learning rates, etc., all follow standard practice in the DL community. The number of fake data training (1000) and the number of MC samples for evaluation (S) are flexible and not tuned.

For λ , we keep it consistent between pre-training and fine-tuning, without elaborated tuning, for example, $\lambda = 2e - 4$ for the wide-ResNet-28-10 architecture on CIFAR-10, $\lambda = 1e - 4$ for ResNet-50 architecture on ImageNet, and $\lambda = 5e - 4$ for MobileNet-V2 architecture on CASIA. These values correspond to isotropic Gaussian priors with σ_0^2 as 0.1, 0.0078, and 0.0041 on CIFAR-10, ImageNet, and CASIA, respectively. It is notable that for a “small” dataset like CIFAR-10, a flatter prior is preferred. While on larger datasets with stronger data evidence, we need a sharper prior for regularization.

For γ , we use $\gamma = 0.75$ for training across all the scenarios. But it is not used for OOD detection in the testing phase. For estimating the results of OOD detection, we use the non-parametric metric average precision (see the experiment setup in Sec 4), which is the Area Under the Precision-Recall Curve and is more suitable than the ROC-AUC metric when there is class imbalance.

For the pre-training, we follow standard protocols available online. On CIFAR-10, we perform CutOut (DeVries & Taylor, 2017) transformation upon popular resize/crop/flip transformation for data augmentation. On ImageNet, we leverage the ResNet-50 checkpoint on PyTorch Hub as the converged deterministic model. On face tasks, we train MobileNetV2 following popular hyper-parameter settings, and the pre-training takes 90 epochs. We use the same weight decay coefficients in both the pre-training and the fine-tuning.

For models on face recognition, we utilize the features be-

fore the last FC layer of the MobileNetV2 architecture to conduct feature distance-based face classification in the validation phase, due to the open-set nature of the validation data. The *Bayes ensemble* is similarly achieved by assembling features from multiple runs as the final feature for estimating predictive performance. But we still adopt the output from the last FC layer for uncertainty estimation (i.e., calculating Eq. (4)).

For *BayesAdapter w/ reg*, the training perturbation budget is identical to the evaluation budget on CIFAR-10 and ImageNet. But we set the budget of the uniform noise used for training in face tasks to be 1/4 of the evaluation budget to make the models more sensitive to the perturbed data. We adopt PGD for generating adversarial samples in the validation phase. Concretely, we attack the *posterior predictive* objective, i.e., Eq. (3), with $S = 20$ MC samples. On CIFAR-10, we set $\delta_m = 0.031$ and perform PGD for 20 steps with step size at 0.003. On ImageNet and face recognition, we set $\delta_m = 16/255$ and perform PGD for 20 steps with step size at 1/255.

Regarding the fake data, we craft 1000 fake samples for training and 10000 ones for evaluation with SNGAN (Miyato et al., 2018) on CIFAR-10; we craft 1000 fake samples for training and 1000 ones for evaluation with BigGAN (Brock et al., 2018) on ImageNet; we randomly sample 1000 fake samples for training and 10000 ones for evaluation from DeepFakes (Deepfakes, 2018), FaceSwap (Faceswap, 2018) and Face2Face (Thies et al., 2016) on face recognition. We perform intensive data augmentation for fake training data with a random strategy including Gaussian blur, JPEG compression, etc.

As for the *MC dropout*, we add dropout-0.3 (0.3 denotes the dropout rate) before the second convolution in the residual blocks in wide-ResNet-28-10, dropout-0.2 after the second and the third convolutions in the bottleneck blocks in ResNet-50, and dropout-0.2 before the last fully connected (FC) layer in MobileNetV2.

For reproducing *Deep Ensemble*, we train 5 *MAPs* separately, and assemble them for prediction and uncertainty quantification. For reproducing *SWAG*, we take use of its official implementation, and leverage 20 MC samples for decision making.

C. More Results for Uncertainty Estimation

We provide the comparison on the quality of uncertainty estimates on face recognition in Table 7 and 8. It is an immediate observation that *BayeAdapter w/ reg* outperforms the extensive baselines significantly, and can detect almost all the OOD instances across the validation datasets. By contrast, *BayeAdapter* and *MAP* are similarly unsatisfactory. Surprisingly, *MC dropout* exhibits some capacity to

Table 7. Comparison on the quality of uncertainty estimates for *adversarial* examples in terms of AP \uparrow on face recognition.

Method	LFW	CPLFW	CALFW	CFP-FF	CFP-FP	VGGFace2	AGEDB-30
<i>MAP</i>	0.191	0.192	0.191	0.211	0.205	0.200	0.199
<i>MC dropout</i>	0.965	0.946	0.959	0.965	0.949	0.954	0.952
<i>BayesAdapter (MFG)</i>	0.232	0.212	0.236	0.242	0.219	0.218	0.216
<i>BayesAdapter (PSE)</i>	0.939	0.746	0.936	0.923	0.667	0.786	0.896
<i>BayesAdapter w/ reg (MFG)</i>	0.998	0.981	0.999	0.999	0.983	0.990	0.995
<i>BayesAdapter w/ reg (PSE)</i>	1.000	1.000	0.999	1.000	1.000	1.000	1.000

 Table 8. Comparison on the quality of uncertainty estimates for *DeepFake* samples in terms of AP \uparrow on face recognition.

Method	LFW	CPLFW	CALFW	CFP-FF	CFP-FP	VGGFace2	AGEDB-30
<i>MAP</i>	0.389	0.456	0.375	0.394	0.454	0.519	0.437
<i>MC dropout</i>	0.846	0.664	0.862	0.874	0.685	0.733	0.785
<i>BayesAdapter (MFG)</i>	0.761	0.520	0.788	0.738	0.441	0.575	0.662
<i>BayesAdapter (PSE)</i>	0.885	0.577	0.899	0.864	0.504	0.675	0.822
<i>BayesAdapter w/ reg (MFG)</i>	0.998	0.987	0.999	0.999	0.986	0.994	0.996
<i>BayesAdapter w/ reg (PSE)</i>	1.000						

detect adversarial instances and DeepFake ones in the face tasks. Comparing these results with those of *MC dropout* on CIFAR-10 and ImageNet, we speculate that such results may stem from the location of deploying dropout in the architecture, which deserves a future investigation.

D. Visualization of Some OOD Data

We provide some random samples of the OOD data used for evaluation in Figure 6. Obviously, these samples are pretty realistic and challenging.

E. Visualization of the Learned Posterior

We plot the parameter posterior of the first convolutional kernel in ResNet-50 architecture learned by *BayesAdapter (MFG)* on ImageNet in Figure 7. The learned posterior variance seems to be disordered, unlike the mean. We leave more explanations as future work.



Figure 6. Some random samples of the OOD data used for evaluation. The first row refers to the fake samples from BigGAN on ImageNet. The second row refers to the adversarial examples generated by PGD on ImageNet. The third row refers to the fake samples from DeepFake.

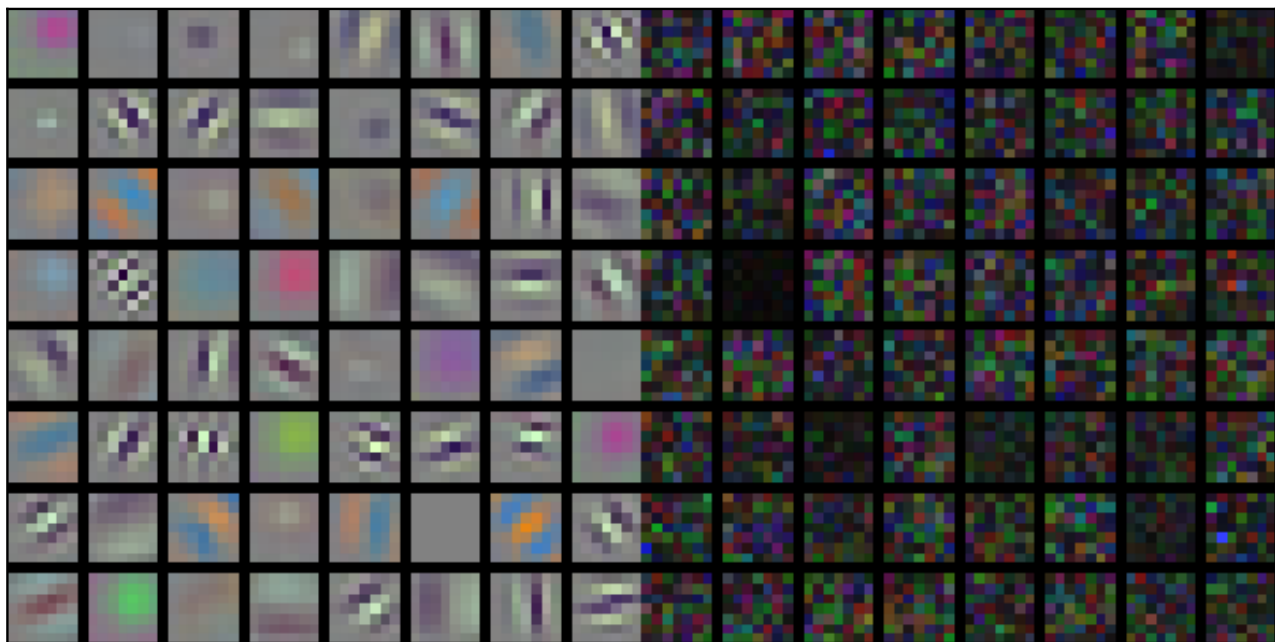


Figure 7. Left: the mean of the *MFG* posterior. Right: the variance of the *MFG* posterior. These correspond to a convolutional kernel with 64 output channels and 3 input channels, where every output channel is plotted as a separate image.